Journal of Colloid and Interface Science **252,** 397–408 (2002)
doi:10.1006/jcis.2002.8450

Spreading of Liquid Drops over Dry Porous Layers: Complete Wetting Case

V. M. Starov,*,[1] S. R. Kostvintsev,* V. D. Sobolev,† M. G. Velarde,‡,§ and S. A. Zhdanov*

*Department of Chemical Engineering, Loughborough University, Loughborough, Lercestershire, LE11 3TU, United Kingdom; †Moscow Institute of Physical Chemistry, 31, Leninsky pr., Moscow 117915, Russian Federation; ‡Instituto Pluridisciplinar, Universidad Complutense, 1, Paseo Juan XXIII, 28040 Madrid, Spain; and §International Center for Mechanical Sciences, Palazzo del Torso, Piazza Garibaldi, Udine 33100, Italy

E-mail: V.M.Starov@lboro.ac.uk; vsobolev@phyche.ac.ru; velarde@fluidos.pluri.ucm.es

Received January 21, 2002; accepted April 30, 2002

Spreading of small liquid drops over thin dry porous layers is investigated from both theoretical and experimental points of view. Drop motion over a porous layer is caused by an interplay of two processes: (a) the spreading of the drop over already saturated parts of the porous layer, which results in an expanding of the drop base; (b) the imbibition of the liquid from the drop into the porous substrate, which results in a shrinkage of the drop base and an expanding of the wetted region inside the porous layer. As a result of these two competing processes, the radius of the drop goes through a maximum value over time. A system of two differential equations is derived to describe the evolution with time of radii of both the drop base and the wetted region inside the porous layer. This system includes two parameters: one accounts for the effective lubrication coefficient of the liquid over the wetted porous substrate and the other is a combination of permeability and effective capillary pressure inside the porous layer. Two additional experiments are used for an independent determination of these two parameters. The system of differential equations does not include any fitting parameter after these two parameters are determined. Experiments were carried out on the spreading of silicone oil drops over various dry microfiltration membranes (permeable in both normal and tangential directions). The time evolution of the radii of both the drop base and the wetted region inside the porous layer are monitored. All experimental data fell on two universal curves if appropriate scales are used with a plot of the dimensionless radii of the drop base and of the wetted region inside the porous layer on dimensionless time. The predicted theoretical relationships are two universal curves accounting quite satisfactorily for the experimental data. According to our theory prediction, (i) the dynamic contact angle dependence on the same dimensionless time as before should be a universal function and (ii) the dynamic contact angle should change rapidly over an initial short stage of spreading and should remain a constant value over the duration of the rest of the spreading process. The constancy of the contact angle on this stage has nothing to do with hysteresis of the contact angle: there is no hysteresis in our system. These conclusions again are in good agreement with our experimental observations.

Key Words: **dry porous layer; capillary spreading; imbibition.**

INTRODUCTION

The spreading of liquids over solid surfaces is a fundamental process with a number of applications in coating, printing, and painting. The spreading over smooth homogeneous surfaces has been considered (1–6). It has been established that singularity at the three-phase contact line is removed by the action of surface forces (5, 6). However, the vast majority of solid surfaces are rough to a different degree and in many cases surfaces are either porous or covered with a thin porous sublayer. The presence of roughness and/or a porous sublayer changes the wettability of the substrate (7) and, hence, the spreading conditions (8–10). The theoretical description of spreading over real surfaces is usually based on an ad hoc empirical "slippage condition" (11–15). In our previous communication to this journal (16), which is referred to as part 1, the spreading of small liquid drops over thin porous layers saturated with the same liquid has been investigated. Instead of the "slippage conditions" Brinkman's equations have been used in part 1 for the description of the liquid flow inside the porous substrate.

In Refs. (8, 9) the flow and imbibition into a porous ribbon circulating in a liquid has been considered. The imbibition into the porous substrate results in the complete disappearance of the film over the distance, which has been determined. The forced aspiration of the liquid drops on the prewetted porous substrates has been experimentally investigated in (10), where the aspiration flux remains constant over the whole drop base. The spreading conditions considered below are very much different from those considered in Refs. (8–10).

In the present work we take up the same problem in the case when a drop spreads over a dry porous layer. The problem is treated below under the lubrication theory approximation and in the case of complete wetting. Spreading of "big drops" (but still small enough to neglect the gravity action) over "thin porous layers" is considered below.

[1] To whom correspondence should be addressed.

0021-9797/02 $35.00

THEORY

The kinetics of liquid motion both in the drop above the porous layer and inside the porous layer itself are taken into account below. The thickness of the porous layer, Δ, is assumed to be much smaller than the drop height, that is, $\Delta \ll h^*$, where h^* is the scale of the drop height. The drop profile is assumed to have a low slope ($h^*/L^* \ll 1$, where L^* is the scale of the drop base) and the influence of the gravity is neglected (small drops, Bond number $\rho g L^{*^2}/\gamma \ll 1$, where ρ, g, and γ are the liquid density, gravity acceleration, and the liquid–air interfacial tension, respectively). That is, only capillary forces are taken into account.

Under such assumptions a system of two differential equations is obtained below to describe the evolution with time of the radius of both the drop base, $L(t)$, and the wetted region inside the porous layer, $l(t)$ (Fig. 1). Further assumptions made are justified in the Appendix.

As in part 1, the profile of axisymmetric drops spreading over the porous substrate (no difference dry or saturated with the same liquid) is governed by the following equation:

$$\frac{\partial h}{\partial t} = u^0 - \frac{1}{r}\frac{\partial}{\partial r}\left\{ r\left[h^3 \frac{\gamma}{3\mu}\frac{\partial}{\partial r}\left(\frac{1}{r}\frac{\partial}{\partial r}\left(r\frac{\partial h}{\partial r}\right) + v^0 h\right)\right]\right\}, \quad [1]$$

Where $h(t, r)$ is the profile of the drop; t and r are the time and the radial coordinate, respectively; $z > 0$ corresponds to the drop and $-\Delta < z < 0$ correspond to the porous layer; $z = 0$ is the drop–porous layer interface (Fig. 1); v and u are the radial and vertical velocity components, respectively; v^0 and u^0 are velocity components at the drop–porous layer interface; μ is the liquid viscosity. The liquid velocity components, v^0 and u^0, on the drop–porous layer interface are calculated below by matching the flow in the drop with the flow inside the porous layer.

The porous layer is very thin and the time for saturation in the vertical direction can be neglected relative to other time scales of the process. Let us calculate the time required for a complete saturation of the porous layer in the vertical direction. According to Darcy's equation,

$$u = \frac{K_p}{\mu}\frac{p_c}{z}, \quad -\Delta < z < 0; \quad u = \frac{dz}{dt},$$

where K_p and P_c are the permeability of the porous layer and the capillary pressure, respectively; z is the position of the liquid front inside the porous layer. The solution of the latter equation results in $\Delta^2 = 2K_p p_c t_\Delta/\mu$, where t_Δ is the time of the complete saturation for the porous layer in the vertical direction and, hence,

$$t_\Delta = \frac{\Delta^2 \mu}{2K_p p_c}.$$

Consideration below is restricted to $t > t_\Delta$. Estimations show that t_Δ is less than t_0, which is the duration of the initial stage of spreading (see part 1 for details and an estimation of t_0. For the capillary spreading regime the only one considered is not applicable at $t < t_0$ Thus, we must consider times such that $t > \max(t_0, t_\Delta)$ when both the initial sage is over and the porous layer is completely saturated in the vertical direction. Accordingly, the porous layer beneath the spreading drop ($0 < r < L(t)$) is always assumed completely saturated.

The capillary pressure inside the porous layer, p_c, can be estimated as

$$p_c \approx \frac{2\gamma}{a^*},$$

where a^* is the scale of capillary radii inside the porous layer. The capillary pressure inside the drop, $p - p_g$, can be estimated as

$$p - p_g \approx \frac{\gamma h^*}{L^{*^2}} = \frac{h^*}{L^*}\frac{\gamma}{L^*} \ll \frac{\gamma}{L^*} \ll \frac{\gamma}{a^*} \approx P_c.$$

The latter means that the capillary pressure inside the pores of the porous layer is several orders of magnitude higher than the capillary pressure in the drop itself.

The boundary conditions for Eq. [1] are as follows:
Symmetry condition in the drop center:

$$\frac{\partial h}{\partial r} = \frac{\partial^3 h}{\partial r^3} = 0, \quad r = 0. \quad [2]$$

Conservation of drop volume:

$$2\pi \int_0^L r h\, dr = V(t). \quad [3]$$

The drop volume changes over time because of the imbibition of the liquid into the porous layer; this means

$$V(t) = V_0 - \pi m \Delta l(t)^2, \quad [4]$$

where V_0 is the initial volume of the drop; m is the porosity of the porous layer; and $l(t)$ is the radius of the wetted circle on the surface of the porous layer. The wetted region is a cylinder with radius $l(t)$ and height Δ. $l(t)$ is referred to below as the radius of the wetted region inside the porous layer.

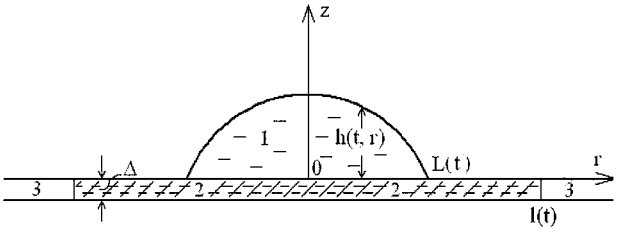

FIG. 1. Cross section of the spreading drop over an initially dry porous substrate with thickness Δ. (1) $L(t)$, radius of the drop base; (2) $l(t)$, radius of the circular edge of the wetted region inside the porous substrate; (3) dry region inside the porous substrate.

Let t_p^* be the time instant when the drop is completely sucked by the porous substrate $V(t_p^*) = 0 = V_0 - \pi m \Delta l^{*^2}$, where l^* is the maximum radius of the wetted region in the porous layer. The latter equation gives.

$$l^* = \left(\frac{V_0}{\pi m \Delta}\right)^{1/2}. \quad [5]$$

l^* is used below to scale the radius of the wetted region in the porous layer, $l(t)$. It is easy to check that the latter equation results in $l^* > L^*$ in our case.

Combination of Eqs. [3] and [4] results in

$$2\pi \int_0^L rh\, dr = V_0 - \pi m \Delta l^2(t). \quad [6]$$

Everywhere at $r < L(t)$ except for a narrow region, ξ, close to the three-phase contact line, we have $h \gg \Delta$, and the liquid motion inside the porous layer under the drop can be neglected both in the vertical and horizontal directions (see the Appendix for details). In this respect our case is considerably different from those considered in (8–10). The size of this narrow region close to the three-phase contact line where suction of liquid from the drop into the porous substrate takes place is estimated in the Appendix.

The latter means that Eq. [1] can be rewritten as

$$\frac{\partial h}{\partial t} = -\frac{\gamma}{3\mu}\frac{1}{r}\frac{\partial}{\partial r}\left\{rh^3\frac{\partial}{\partial r}\left(\frac{1}{r}\frac{\partial}{\partial r}\left(r\frac{\partial h}{\partial r}\right)\right)\right\}, \quad r < L(t) - \xi. \quad [7]$$

Equation [7] should be solved with boundary conditions [2], [6], and

$$h(t, L - \xi) \approx 0. \quad [8]$$

Following the arguments developed in Ref. (6), the solution of Eq. [7] can be obtained using "outer" and "inner" solutions. The outer solution can be deduced in the following way: the left-hand side of Eq. [7] should be set to zero. After integration of the resulting equation with boundary conditions [2], [6], and [8], the "outer" solution becomes

$$h(t, r) = \frac{2V}{\pi L^4}(L^2 - r^2), \quad r < L(t) - \xi. \quad [9]$$

Equation [9] shows that the drop surface profile remains spherical during the spreading process except for a short initial stage, when the porous layer is not saturated, and a final stage, when condition $\Delta \ll h$ is violated everywhere over the whole profile of the drop.

Equation [9] gives the following value of the dynamic contact angle, θ ($\tan\theta \approx \theta$):

$$\theta = \frac{4V}{\pi L^3}, \quad [10]$$

or else

$$L = \left(\frac{4V}{\pi\theta}\right)^{1/3}. \quad [11]$$

The drop motion is a superposition of two motions: (a) the spreading of the drop over the already saturated part of the porous layer, which results in an expansion of the drop base, and (b) a shrinkage of the drop base caused by the imbibition into the porous layer. Hence, we can write the following equation,

$$\frac{dL}{dt} = v_+ - v_-, \quad [12]$$

where v_+ and v_- are unknown velocities of the expansion and the shrinkage of the drop base, respectively.

Let us take the time derivative of both sides of Eq. [11]. It gives

$$\frac{dL}{dt} = -\frac{1}{3}\left(\frac{4V}{\pi\theta^4}\right)^{1/3}\frac{d\theta}{dt} + \frac{1}{3}\left(\frac{4}{\pi V^2\theta}\right)^{1/3}\frac{dV}{dt}. \quad [13]$$

Over the whole duration of the spreading over the porous layer, both the contact angle and the drop volume can only decrease with time. Accordingly, the first term in the right-hand side of Eq. [13] is positive and the second one is negative.

A comparison of the latter two equations yields

$$v_+ = -\frac{1}{3}\left(\frac{4V}{\pi\theta^4}\right)^{1/3}\frac{d\theta}{dt} > 0,$$
$$v_- = -\frac{1}{3}\left(\frac{4}{\pi V^2\theta}\right)^{1/3}\frac{dV}{dt} > 0. \quad [14]$$

There are two substantially different characteristic time scales in our problem: $t_\mu^* \ll t_p^*$, where t_μ^* and t_p^* are time scales of the viscous spreading and the imbibition into the porous layer, respectively;

$$\lambda = \frac{t_\mu^*}{t_p^*} \ll 1$$

is a smallness parameter (around 0.08 under our experimental conditions, see below). Both time scales are calculated below. Then we have $L = L(T_\mu, T_p)$ (17), where T_μ is a fast time of the viscous spreading and T_p is a slow time of the imbibition into the porous substrate. The time derivative of $L(T_\mu, T_p)$ is

$$\frac{dL}{dt} = \frac{\partial L}{\partial T_\mu} + \lambda\frac{\partial L}{\partial T_p}. \quad [15]$$

A comparison of Eqs. [12], [14], and [15] shows that

$$v_+ = \frac{\partial L}{\partial T_\mu} = -\frac{1}{3}\left(\frac{4V}{\pi\theta^4}\right)^{1/3}\frac{d\theta}{dt},$$
$$v_- = -\lambda\frac{\partial L}{\partial T_p} = -\frac{1}{3}\left(\frac{4}{\pi V^2\theta}\right)^{1/3}\frac{dV}{dt}.$$

The smallness

$$\lambda = \frac{t_\mu^*}{t_p^*} \ll 1$$

means that in the case under consideration two processes go actually independently: the spreading of the drop over the saturated part of the porous layer and the shrinkage of the drop base caused by the imbibition of the liquid from the drop into the porous layer.

The decrease of the drop volume, V, with time is determined solely by the imbibition into the porous substrate and, hence, the drop volume, V, only depends on the slow time scale.

According to the previous consideration, the whole spreading process can be subdivided into two stages:

(i) A first fast stage, when the imbibition into the porous substrate can be neglected, and the drop spreads with approximately constant volume. This stage goes in the same way as the spreading over a saturated porous layer and the arguments developed in part 1 can be used here again.

(ii) A second slow stage, when the spreading process already is almost over and the evolution is determined by the imbibition into the porous substrate.

During the first stage Eq. [34] from part 1 can be rewritten in the following form,

$$L(t) = \left[\frac{10\gamma\omega}{\mu}\left(\frac{4V}{\pi}\right)^3\right]^{0.1}(t+t_0)^{0.1}, \qquad [16]$$

where t_0 is the duration of the initial stage of spreading when the capillary regime of spreading is not applicable; ω is an effective lubrication parameter, which has been discussed and estimated in part 1. It is important to emphasize that the effective lubrication parameter, ω, is independent of the drop volume (16) and depends solely on the porous layer properties. According to Eq. [16], the characteristic time scale of the first stage of spreading is

$$t_\mu^* = \frac{\mu L_0}{10\gamma\omega}\left(\frac{\pi L_0^3}{4V_0}\right)^3, \qquad [17]$$

where $L_0 = L(t_0)$.

Combination of Eqs. [10] and [16] gives

$$\theta = \left(\frac{4V}{\pi}\right)^{0.1}\left(\frac{\mu}{10\gamma\omega}\right)^{0.3}(t+t_0)^{-0.3}.$$

Substitution of the latter expression into the first, Eq. [14], gives the following expression for the velocity of the drop base expansion, v_+:

$$v_+ = 0.1\left(\frac{4V}{\pi}\right)^{0.3}\left(\frac{10\gamma\omega}{\mu}\right)^{0.1}\frac{1}{(t+t_0)^{0.9}}. \qquad [18]$$

Substitution of Eq. [4] into the second Eq. [14] gives the following expression for velocity of the drop base shrinkage, v_-:

$$v_- = \frac{2\pi^{2/3}m\Delta l}{3}\left(\frac{4}{(V_0-\pi m\Delta l^2)^2\theta}\right)^{1/3}\frac{dl}{dt}. \qquad [19]$$

Substitution of the latter two equations into Eq. [13] results in

$$\frac{dL}{dt} = 0.1\left(\frac{4V}{\pi}\right)^{0.3}\left(\frac{10\gamma\omega}{\mu}\right)^{0.1}\frac{1}{(t+t_0)^{0.9}} - \frac{2\pi^{2/3}m\Delta l}{3}\left(\frac{4}{(V_0-\pi m\Delta l^2)^2\theta}\right)^{1/3}\frac{dl}{dt}. \qquad [20]$$

The only unknown function now is the radius of the wetted region inside the porous layer, $l(t)$, which is determined below.

Inside the Porous Layer Outside the Drop ($-\Delta < z < 0$, $L < r < l$)

The liquid flow inside the porous layer obeys the Darcy equation:

$$\frac{1}{r}\frac{\partial}{\partial r}\left(r\frac{\partial p}{\partial r}\right) = 0, \quad v = -\frac{K_p}{\mu}\frac{\partial p}{\partial r}.$$

Solution of the latter equations is

$$p = -(A\mu/K_p)\ln r + B, \qquad v = \frac{A}{r}, \qquad [21]$$

where A and B are integration constants, which should be determined using the boundary conditions for the pressure at the drop edge, $r = L(t)$, and at the circular edge of the wetted region inside the porous layer, $r = l(t)$. The latter boundary condition is

$$p = p_g - p_c, \quad r = l(t), \qquad [22]$$

where

$$p_c \approx \frac{2\gamma}{a^*}$$

is the capillary pressure inside the pores of the porous layer and a^* is a characteristic scale of the pore radii inside the porous layer.

The boundary condition at the drop edge is

$$p = p_g + p_d, \quad r = L(t), \qquad [23]$$

where p_d is an unknown pressure. It is shown below that $p_d \ll p_c$. However, we keep this small value for a future estimation.

Taking into account the latter two boundary conditions, both integration constants, A and B, can be determined, which gives the following expression for the radial velocity according to

Eq. [21]:

$$\upsilon = \frac{K_p(p_c + p_d)/\mu}{r \ln \frac{l}{L}}. \quad [24]$$

The velocity at the circular edge of the wetted region inside the porous layer is

$$\frac{dl}{dt} = \upsilon|_{r=l}$$

Combination of the latter two equations gives the evolution equation for $l(t)$:

$$\frac{dl}{dt} = \frac{K_p(p_c + p_d)/\mu}{l \ln \frac{l}{L}}. \quad [25]$$

An estimation of the time scale t_p^* can be made according to Eq. [25] and taking into account Eq. [5],

$$\frac{l^*}{t_p^*} \approx \frac{K_p p_c/\mu}{l^* \ln \frac{l^*}{L^*}}$$

or

$$t_p^* \approx \frac{l^{*^2} \ln \frac{l^*}{L^*}}{K_p p_c/\mu} = \frac{V_0 \ln \frac{l^*}{L^*}}{\pi m \Delta K_p p_c/\mu}. \quad [26]$$

A comparison of the estimated values of t_μ^* according to Eq. [17] and of t_p^* according to Eq. [26] shows that under all our experimental conditions (see below) the inequality $t_\mu^* \ll t_p^*$ is satisfied.

Omission of the small term, p_d, and substitution of Eq. [25] into Eq. [20] gives the following system of differential equations for the evolution of both the radius of the drop base, $L(t)$, and that of the wetted region inside the porous layer, $l(t)$:

$$\frac{dL}{dt} = 0.1\left(\frac{4(V_0 - \pi m \Delta l^2)}{\pi}\right)^{0.3}\left(\frac{10\gamma\omega}{\mu}\right)^{0.1}\frac{1}{(t+t_0)^{0.9}} - \frac{2\pi m \Delta K_p p_c L/\mu}{3(V_0 - \pi m \Delta l^2)\ln \frac{l}{L}}, \quad [27]$$

$$\frac{dl}{dt} = \frac{K_p p_c/\mu}{l \ln \frac{l}{L}}. \quad [28]$$

Let us make the system of differential equations [27] and [28] dimensionless using new scales $\bar{L} = L/L_m$, $\bar{l} = l/l^*$, and $\bar{t} = t/t_p^*$, where L_m is the maximum value of the drop base, which is reached at the time instant t_m. The same symbols are used for the dimensionless variable as for corresponding dimensional variables (marked with an overbar). The system of equations. [27] and [28] transforms as

$$\frac{d\bar{L}}{d\bar{t}} = \frac{2}{3}\frac{(\bar{t}_m + \bar{\tau})^{0.9}}{\left(1 - \bar{l}_m^2\right)^{1.3}(1 + \bar{\chi}\ln \bar{l}_m)}\frac{(1-\bar{l}^2)^{0.3}}{(\bar{t}+\bar{\tau})^{0.9}} - \frac{2}{3}\frac{\bar{L}}{(1-\bar{l}^2)\left(1 + \bar{\chi}\ln \frac{\bar{l}}{\bar{L}}\right)}, \quad [29]$$

$$\frac{d\bar{l}}{d\bar{t}} = \frac{1}{\bar{l}\left(1 + \bar{\chi}\ln \frac{\bar{l}}{\bar{L}}\right)}, \quad [30]$$

where

$$\bar{\tau} = t_0/t_p^* \ll 1 \quad \text{and} \quad \bar{\chi} = 1/\ln\frac{l^*}{L_m}.$$

Thus, the latter system includes only two dimensionless parameters, $\bar{\tau}$ and $\bar{\chi}$; the first one is very small and the second one changed insignificantly under our experimental conditions because of a weak logarithmic dependence on l^*/L_m.

Accordingly, the two dimensionless dependencies, $\bar{L}(\bar{t})$ and $\bar{l}(\bar{t})$, should fall on two almost universal curves, which is in very good agreement with our experimental observations (see Results and Discussion).

According to Eq. [29], the dimensionless velocities of the expansion of the drop base, $\bar{v}_+$, and the shrinkage, $\bar{v}_-$, are

$$\bar{v}_+ = \frac{2}{3}\frac{(\bar{t}_m + \bar{\tau})^{0.9}}{\left(1 - \bar{l}_m^2\right)^{1.3}(1 + \bar{\chi}\ln \bar{l}_m)}\frac{(1-\bar{l}^2)^{0.3}}{(\bar{t}+\bar{\tau})^{0.9}},$$

$$\bar{v}_- = \frac{2}{3}\frac{\bar{L}}{(1-\bar{l}^2)\left(1 + \bar{\chi}\ln \frac{\bar{l}}{\bar{L}}\right)}. \quad [31]$$

Figure 2 shows dimensionless velocity $\bar{v}_+$ and $\bar{v}_-$ calculated according to Eqs. [31]. It appears that

(a) the first stage is very short. The capillary spreading prevails on this stage over the drop base shrinkage caused by the liquid imbibition into the porous substrate;

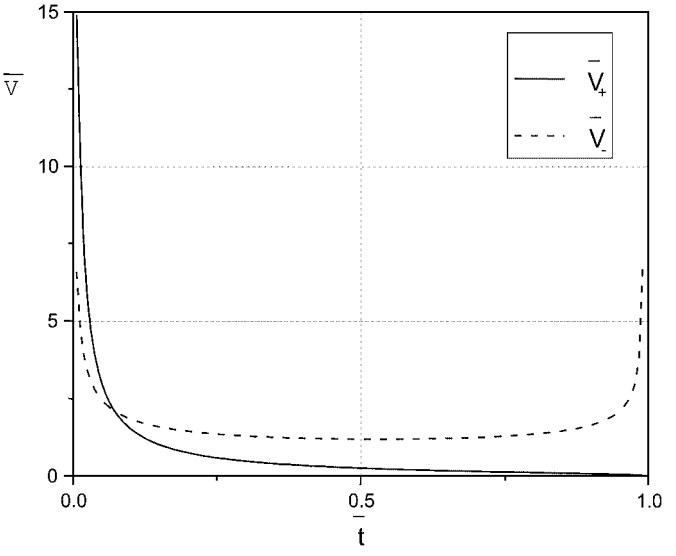

FIG. 2. Dimensionless velocity of spreading ($\bar{v}_+$, solid line) and velocity of drop shrinkage ($\bar{v}_-$, dotted line) on dimensionless time, calculated according to Eq. [31]. Intersection of these two dependencies determines the value of the dimensionless time $\bar{t}_m \approx 0.08$ when the radius of the drop base reaches its maximum value $\bar{L}_m = 1$ (in dimensionless units).

(b) the spreading of the drop almost stops after the first stage of spreading and the shrinkage of the drop base is determined by the suction of the liquid from the drop into the porous substrate.

Let us consider the asymptotic behavior of the system [27] and [28] over the the second stage of the spreading. According to Fig. 2, over the second stage of the spreading, the velocity of the expansion of the drop, v_+, decreases. To understand the asymptotic behavior, the term corresponding to v_+ in the left-hand side of Eq. [27] is omitted. This gives

$$\frac{dL}{dt} = -\frac{2\pi m\Delta K_p p_c L/\mu}{3(V_0 - \pi m\Delta l^2)\ln\frac{l}{L}}, \qquad [32]$$

while the second, Eq. [28], is left unchanged. The system of differential equations [28] and [32] can be solved analytically. For this purpose Eq. [32] is divided by Eq. [28], which gives

$$\frac{dL}{dl} = -\frac{2\pi m\Delta L l}{3(V_0 - \pi m\Delta l^2)}$$

If $V = V_0 - \pi m\Delta l^2$ is used instead of l, the latter equation takes the following form:

$$\frac{dL}{dV} = \frac{L}{3V},$$

which can be easily integrated and the solution is

$$V = CL^3, \qquad [33]$$

where C is an integration constant. Let us rewrite Eq. [10] using the same dimensionless variables:

$$\bar{V} = \frac{4L_m^3}{\pi V_0}\theta\bar{L}^3. \qquad [34]$$

A comparison of Eqs. [33] and [34] shows that the dynamic contact angle asymptotically remains constant in the second stage. This constant value is marked below as θ_e. Let us introduce

$$\theta_m = \frac{\pi V_0}{4L_m^3}\left(1 - \bar{l}_m^2\right),$$

which is the value of the dynamic contact angle at the time instant when the maximum value of the drop base is reached. Then Eq. [34] can be rewritten as

$$\frac{\theta}{\theta_m} = \frac{(1-\bar{l}^2)/(1-\bar{l}_m^2)}{\bar{L}^3} \qquad [35]$$

and the latter relationship should be a universal function of the dimensionless time, $\bar{t}$. This conclusion agrees well with our experimental observations (see Results and Discussion). It is necessary to emphasize that in the case under consideration the constancy of the contact angle has nothing to do with the contact angle hysteresis: there is no hysteresis in our system here. θ_e is not a receding contact angle (as in Ref. (10)) but forms as a result of a self-regulation of the flow in the drop–porous layer system.

The system of equations [27] and [28] includes seven parameters, five of which can be measured directly (V_0, γ, μ, m, and Δ are the initial volume of the drop, the liquid–air interfacial tension, the liquid viscosity, the porosity of the porous layer, and the thickness, respectively), and two additional parameters, ω and $K_p p_c$, which should be determined independently. It is noteworthy that the porous layer permeability and the capillary pressure always enter as a product; that is, this product can be considered as a single parameter. A procedure of independent determination of an effective lubrication coefficient, ω, was discussed in part 1.

EXPERIMENTAL

Silicone oils SO20 (viscosity 0.218 P), SO50 (viscosity 0.554 P), SO100 (viscosity 1.18 P), and SO500 (viscosity 5.582 P) purchased from PROLABO were used in the spreading experiments. The viscosity of oils were measured using the capillary Engler Viscometer VPG-3 at $20 \pm 0.5^\circ$C. Cellulose nitrate membrane filters, purchased from Sartorius (type 113), with pore size $a = 0.2$ μm and $a = 3$ μm (marked by the supplier) were used as porous layers. These membranes are referred to below as the membrane $a = 0.2$ μm and the membrane $a = 3$ μm, respectively. Pore size distribution and permeability of membranes were tested using the Coulter Porometer II.

The pore size of the membrane $a = 0.2$ μm fell in the range 0.2–0.38 μm, with the average pore size 0.34 μm. The permeability of the same membrane is equal to 12 L/(min cm^2) (air flux at the transmembrane pressure 5 bar). The permeability of the membrane $a = 3$ μm is 2.5 L/(min cm^2) at the transmembrane pressure 0.1 bar. All membrane samples used are plane parallel circles of radius 25 mm and thickness in the range from 0.0130 to 0.0138 cm. The porosity of the membranes ranges between 0.65 and 0.87. The porosity was measured using the difference in the weight of saturated-with-oil and dry membranes. Membranes were dried for 3–5 h at 95°C and then stored in a dry atmosphere prior to the spreading experiments.

Figure 3 shows the sample chamber for monitoring the spreading of drops over initially dry porous layers. The time evolution

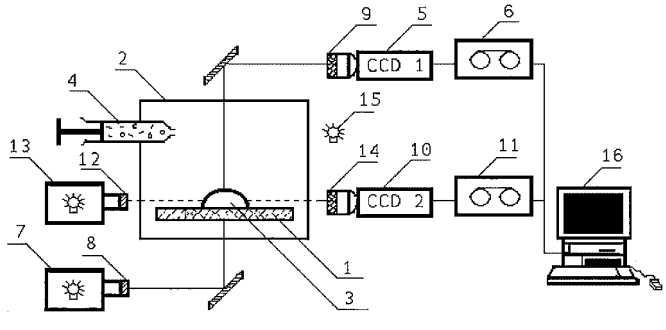

FIG. 3. Schematic presentation of the experimental setup (see explanations in Experimental).

of the radius of the drop base, $L(t)$, the dynamic contact angle, $\theta(t)$, and the radius of the wetted region inside the porous layer, $l(t)$, were monitored. The porous wafer (1) (Fig. 3), was placed in a thermostated and hermetically closed chamber (2), where zero humidity and fixed temperature ($20 \pm 0.5^{\circ}$C) were maintained. To prevent temperature fluctuations, the chamber was made from brass. In the chamber walls several channels were drilled, which were used for pumping a thermostating liquid. The chamber was equipped with a fan. The temperature was monitored by a thermocouple. A box with a dried silica gel was used to keep zero humidity inside the chamber. Droplets of the liquid under investigation (3) were placed onto the wafer by a dosator (4) (Fig. 3). The distance from the wafer to the tip of the dosator ranged from 0.5 to 1 cm in different experiments. The volume of drops was set by the diameter of the separable capillary of the dosator in the range 1–15 μl.

The chamber is equipped with optical glass windows for observation of both the shape and the size of the spreading drops: a side view and a top view were carried out. Two CCD cameras and two tape recorders were used for storing the sequences of the spreading. Different colors of monochromatic light were used for side and top views to eliminate a spurious illumination of images. An optical circuit for top view (illuminator (7) and camera (5) was equipped with interferential light filters (8, 9) with a wavelength of 520 nm. A side-view circuit (illuminator (13) and camera (10) were equipped with filters (12, 14) with a wavelength of 640 nm. Such an arrangement suppresses illumination of the CCD camera (2) by a scattered light from the membrane and, hence, results in higher precision of the measurements. Automatic processing of images was carried out using an image processor, "Scion Image." A discretization of time in the processing ranged from 0.1 to 10 s in different experiments; the size of pixel in an image was 0.01–0.05 mm in different runs.

Experiments were carried out in the following order:

- the membrane was placed in the chamber and left in a dry atmosphere for 15–30 min,
- a light pulse produced by a flash gun was used to synchronize the time instant when the drop started to spread and both videotape recorders (a side view and a view from above), and
- a droplet of silicone oil was placed onto the membrane.

Each run was carried out until complete imbibition of the drop into the membrane took place.

Independent Determination of $K_p p_c$

As mentioned above, the permeability of the porous layer and the capillary pressure always enter as a product, i.e., as a single coefficient. Additional experiments were carried out to determine this coefficient. For this purpose the horizontal imbibition of the liquid under investigation into the dry porous sheet was undertaken. Rectangular sheets 1.5 cm × 3 cm were used. Those porous sheets were cut from the same membranes used in the spreading experiments. Each sheet was immersed to a depth of 0.3–0.5 cm into a liquid container and the position of the imbibition front was monitored over time. In the case under investigation a unidirectional flow of liquid inside the porous substrate took place. Using Darcy's law, we can conclude that

$$d^2(t) = 2K_p p_c t/\mu, \qquad [36]$$

where $d(t)$ is the position of the imbibition front inside the porous layer. It was found that in all runs $d^2(t)/2$ proceeds along a straight line, whose slope gives us the $K_p p_c$ value. According to (18), $K_p p_c$ should be independent of the tested liquid viscosity.

The measured values of $K_p p_c$ are presented in Table 1.

TABLE 1

Membrane pore size (μm)	Liquid	$K_p p_c$ (dyn)
3	SO20	$(1.2 \pm 0.4) \times 10^{-4}$
3	SO100	$(1.77 \pm 0.03) \times 10^{-4}$
3	SO500	$(1.6 \pm 0.2) \times 10^{-4}$
0.2	SO5	$(3.4 \pm 0.3) \times 10^{-5}$
0.2	SO100	$(3.1 \pm 0.3) \times 10^{-5}$

Table 1 shows that coefficient, $K_p p_c$, for each type of membrane is independent of the tested liquid within the experimental error. Averaged values of $K_p p_c$ for each membrane were used in the calculations.

RESULTS AND DISCUSSION

According to our observations, the whole spreading process can be subdivided into two stages (see Fig. 4 as an example): fast spreading over the first several seconds until the maximum radius, L_m, of the drop base is reached. Over the duration of the first stage an imbibition front inside the membrane expands slightly ahead of the spreading drop. After that the drop base starts to shrink slowly and the imbibition front expands until the drop completely disappears. An example of the time evolution of the radius of the drop base and the radius of the wetted region inside the porous layer is provided in Fig. 5.

In all our spreading experiments, the drops remain spherical over the duration of both the first and the second stages of the spreading process. This was cross-checked by reconstruction of the drop profiles at different time instants of spreading, fitting those profiles by a spherical cap,

$$h = z_{center} + \sqrt{R^2 - (r - r_{center})^2},$$

where (r_{center}, z_{center}) is the position of the center of the sphere and R is the radius of the sphere. r_{center}, z_{center}, and R are used as fitting parameters. The fitting is based on the Levenberg–Marquardt algorithm. In all cases the reduced χ^2 value is found to be less than 10^{-4}. The fitted parameter R gives the radius of curvature of the spreading drops at different times.

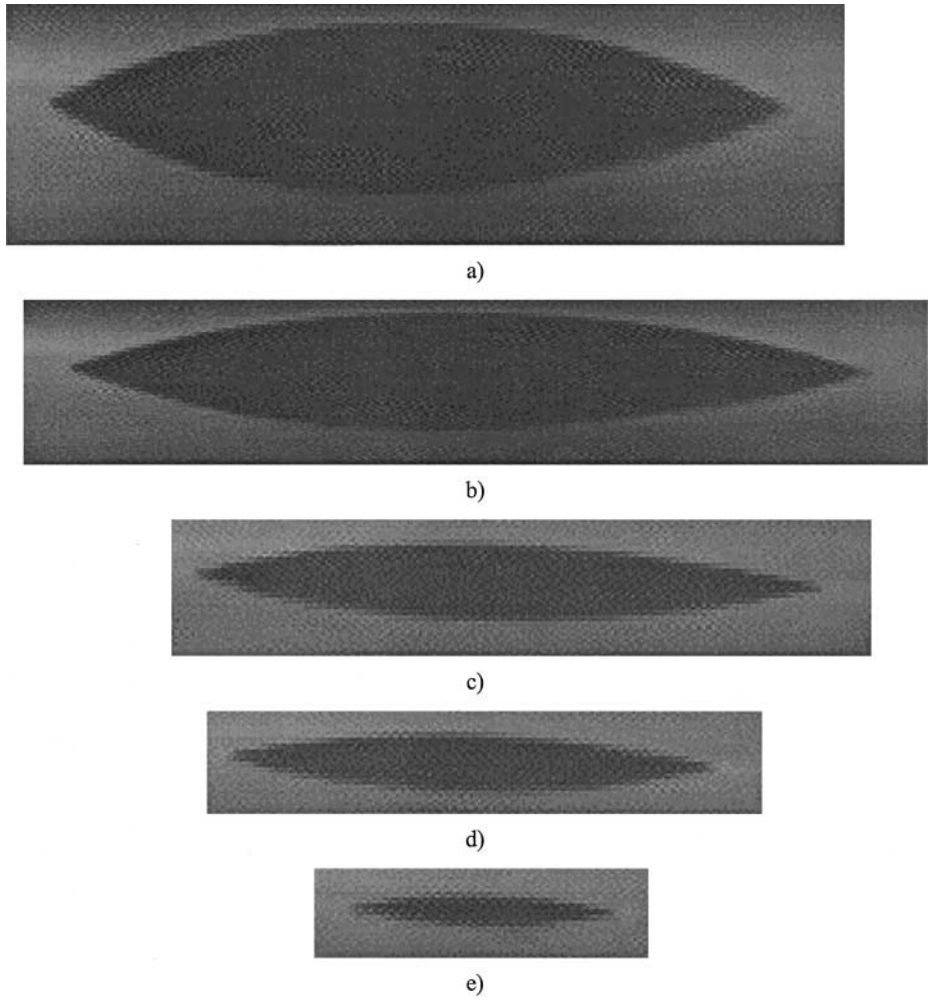

FIG. 4. Time sequence of the spreading of SO500, volume 8.7 μl over the membrane with pore size 3 μm (side view): (a) $t = 0.5$ s (after deposition); (b) 3 s; (c) 12 s; (d) 22 s; (e) 36 s.

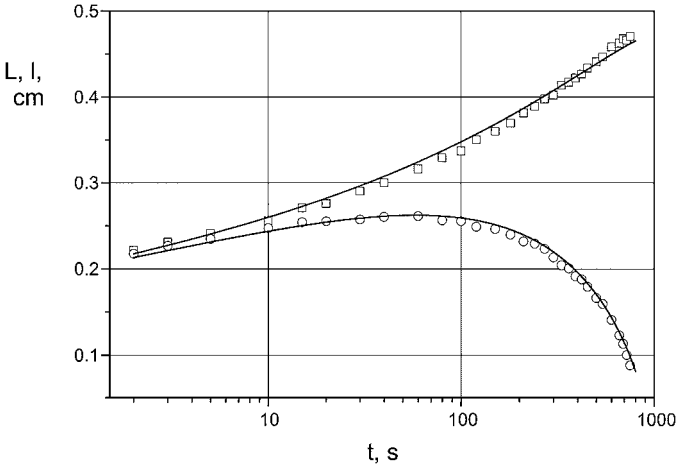

FIG. 5. Development over time of the drop base, L, and the radius of the wetted region inside the porous layer, l. The same drop as in Fig. 4: SO500 drop, placed onto the membrane with pore size 3 μm. Solid lines calculated according to Eqs. [27] and [28].

The edge of the wetted region inside the porous layers was always circular. Drops remained in the center of this circle over the duration of the spreading process. No deviations from cylindrical symmetry or instabilities were detected.

The spherical form of the spreading drop allows measuring the evolution of the dynamic contact angle of the drop. In all cases the dynamic contact angle decreases very fast over the first stage of spreading until a constant value is reached, which is refereed to below as θ_e. The dynamic contact angle remains constant, θ_e, over the main part of the second stage.

An example of the evolution with time of the dynamic contact angle is presented in Fig. 6. for the same drop as in Fig. 4 and Fig. 5. Figure 6 shows that the dynamic contact angle decreases fast over the duration of the first stage of the spreading when the radius of the drop base expands to its maximum value, L_m. The dynamic contact angle remains almost unchanged over the duration of the second stage of spreading. Note again that this behavior has nothing to do with the hysteresis of the contact angle because the latter does not occur in our system: silicone

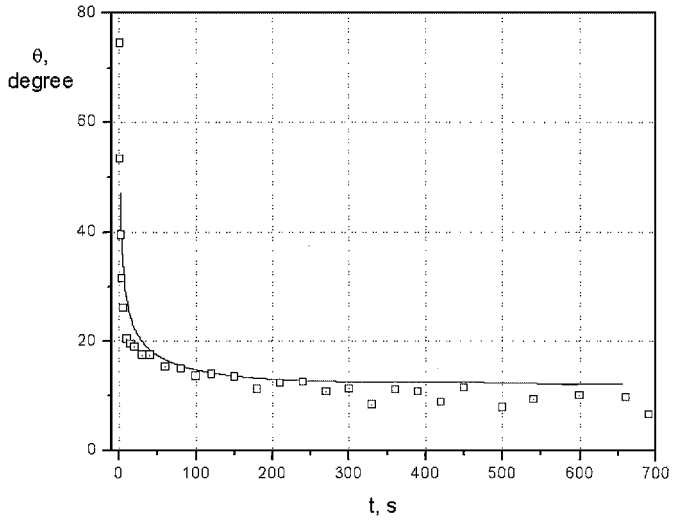

FIG. 6. Development over time of the dynamic contact angle. The same drop as in Figs. 4 and 5: SO500 drop, placed onto the membrane with pore size 3 μm. Solid line calculated according to Eqs. [27] and [28].

oils on nitrate cellulose membranes. Solid lines in Figs. 5 and 6 represent the results of numerical integration of the system of equations [27] and [28]. The rkf45 numerical algorithm was used for calculations. The short final period (just before the drop disappears) is not covered by our calculations. Close to this final stage the calculation errors increased, which was caused by a division by a very small quantity in the second term in the right-hand side of Eq. [27].

Table 2 shows that the final value of the dynamic contact angle, θ_e (last column in Table 2), depends on the volume of the drop as well as on the viscosity of the liquid and, hence, θ_e is determined solely by hydrodynamics.

Figure 7a presents experimentally measured dependencies of radius of the drop base and the wetted region inside the porous layer on time for different silicone oils, porous layers, and drop volumes. All relevant values are summarized in Table 2. The main result appears in Fig. 7b, which shows that all experimental data (the same as in Fig. 7a) fall on two universal curves if dimensionless coordinates are selected as follows:

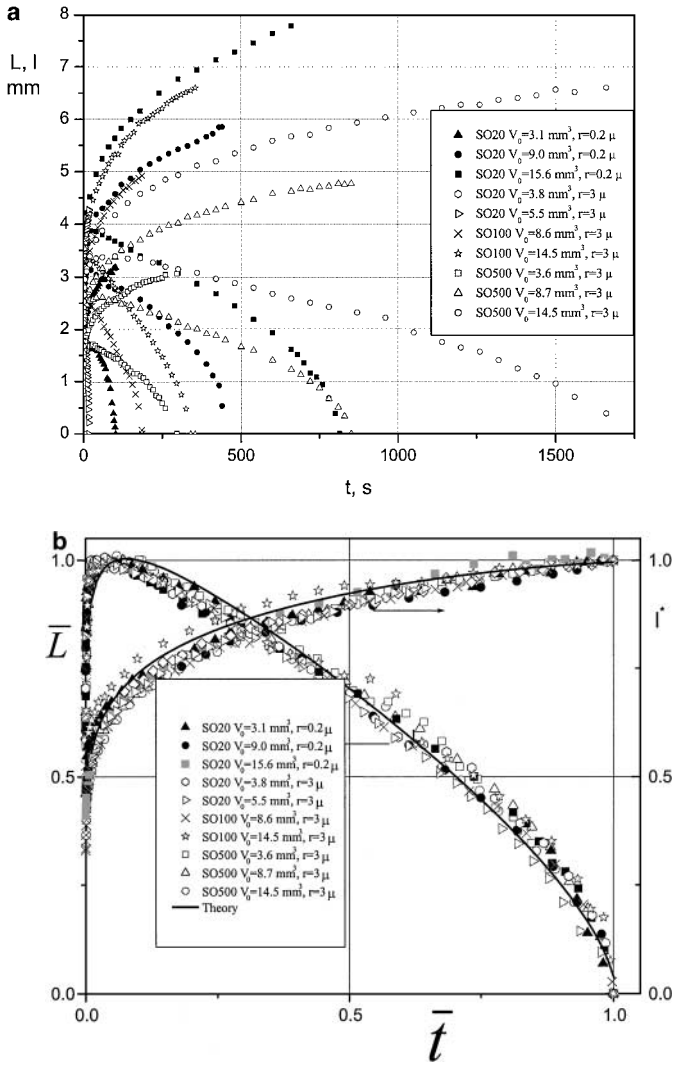

FIG. 7. (a) Measured dependencies of radii of the drop base (L, mm) and radii of the wetted region inside the porous layer (l, mm) on time (t, s). All relevant values are summarized in Table 2. (b) The same as in Fig. 7a but using dimensionless coordinates: $\bar{L} = L/L_m$, $\bar{l} = l/l^*$, $\bar{t} = t/t_p^*$, where L_m is the maximum value of the drop base, which is reached at the moment t_m. The same symbols (with overbar) are used for dimensionless values as for dimensional ones. l^* and t_p^* according to Eq. [5] and Eq. [26], respectively. Solid lines according to Eqs. [29] and [30].

TABLE 2

Liquid	Notataion on figures	Membrane pore size (μm)	V_0 (m1 × 10^3)	Δ (mm)	m-porosity	t_p^* (s)	l^* (cm)	l^* (theory)	L_m (cm)	L_m (theory)	θ_m (deg)	θ_e (deg)
SO20	▲	0.2	3.1	0.114	0.85	102	0.318	0.317	0.179	0.184	20.0	12
SO20	●	0.2	9.0	0.116	0.72	440	0.585	0.584	0.314	0.31	12.6	11.4
SO20	■	0.2	15.6	0.116	0.73	814	0.77	0.766	0.387	0.39	14.2	12.1
SO20	⬡	3	3.8	0.136	0.87	10.9	0.345	0.319	0.196	0.198	25.9	22.3
SO20	▷	3	5.5	0.134	0.83	17.1	0.428	0.398	0.223	0.234	20.3	18.6
SO100	×	3	8.6	0.137	0.82	186	0.493	0.494	0.257	0.274	18.5	11
SO100	☆	3	14.5	0.138	0.77	354	0.659	0.659	0.332	0.34	15.5	17.2
SO500	□	3	3.6	0.138	0.89	296	0.306	0.306	0.174	0.179	22.6	19.4
SO500	△	3	8.7	0.138	0.88	851	0.477	0.478	0.264	0.286	19.1	17.3
SO500	○	3	14.5	0.136	0.78	1660	0.66	0.660	0.339	0.34	15.8	16.5

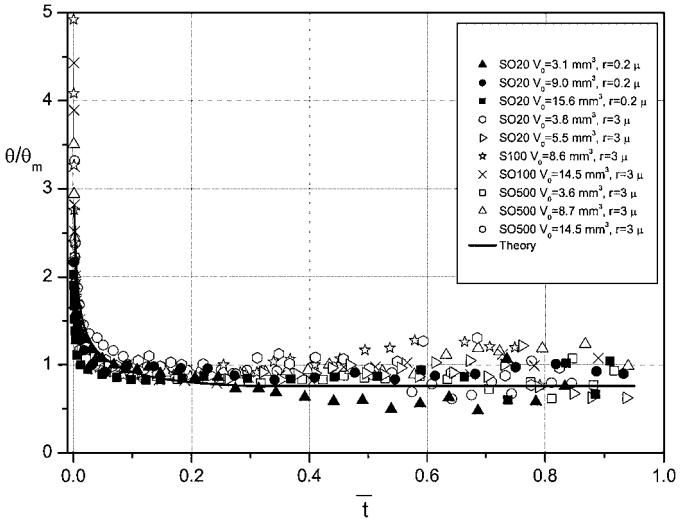

FIG. 8. Dynamic contact angle on the dimensionless time. Solid line according to Eq. [35].

$\bar{L} = L/L_m$, $\bar{l} = l/l^*$, and $\bar{t} = t/t_p^*$, where L_m is the maximum value of the drop base, which is reached at the time instant t_m. The same symbols (with and over bar) are used for dimensionless values as for dimensional. The scale l^* is determined by Eq. [5] and the time scale t_p^* is given by Eq. [26].

The measured values of L_m, l^*, and t_p^* for all experimental runs are given in Table 2. Figure 7b shows that the dimensionless time $\bar{t}_m$ is about $0.08 \approx \lambda \ll 1$, as was stated above. The dimensionless time 1 corresponds to the time instant when the drop is completely sucked by the porous substrate. Solid curves on Fig. 7b represent the solution of the system of differential equations [29] and [30]. If the parameters $\bar{\tau}$ and $\bar{\chi}$ change, then both those theoretical curves remain inside the array of experimental points. In this sense they represent universal relationships.

The twelfth column in Table 2 gives the experimental values of the dynamic contact angle, θ_m, which the drop has when the drop base reaches its maximum value, L_m. These values were used for plotting the time evolution of the dynamic contact angle, θ/θ_m. Figure 8 shows that all experimental points fall on a single universal curve, as predicted by Eq. [35].

The solid line in Fig. 8 is a result of calculations according to Eq. [35], where dimensionless dependencies $\bar{L}(\bar{t})$ and $\bar{l}(\bar{t})$ are taken from the previous Fig. 7b.

APPENDIX 1

The slip boundary condition (10–14) is used below for simplicity. The slippage coefficient is taken from (16). Similar results can be deduced using Brinkman's equations for the description of the liquid flow inside porous layers.

The slippage condition at the drop–porous layer interface is

$$\mu \frac{\partial v}{\partial z}\bigg|_{z=+0} = \mu_p \frac{v^0 - v_p}{\delta}, \qquad [A.1]$$

where

$$v_p = \frac{K_p}{\mu_p}\frac{\partial p_p}{\partial r}$$

is the velocity inside the porous substrate; μ_p is an effective viscosity inside the porous layer (18), and $p_g - p_p$ is the pressure inside the porous layer, which may be different from the pressure in the spreading drop. The porous layer thickness, Δ, is assumed to be much bigger than the Brinkman's length,

$$\delta = \sqrt{K_p}.$$

Hence, both velocities v^0 and u^0 change stepwise at the drop–porous layer interface: the jump of the first velocity is given by Eq. [A.1], while the jump of the second velocity is

$$u^0 = -\frac{K_p}{\mu_p \delta}\left(-\frac{\gamma}{r}\frac{\partial}{\partial r}\left(r\frac{\partial h}{\partial r}\right) + p_p\right). \qquad [A.2]$$

The latter means that the vertical velocity changes stepwise from the value given by Eq. [A.2] on the drop–porous layer interface to zero inside the porous layer. Equation [A.1] becomes

$$v^0 = \frac{K_p}{\mu_p}\frac{\partial p_p}{\partial r} + \frac{\delta h \gamma}{\mu_p}\frac{\partial}{\partial r}\left(\frac{1}{r}\frac{\partial}{\partial r}\left(r\frac{\partial h}{\partial r}\right)\right). \qquad [A.3]$$

Substitution of Eqs. [A.2] and [A.3] into Eq. [1] gives

$$\frac{\partial h}{\partial t} = \frac{K_p}{\mu_p \delta}\left(\frac{\gamma}{r}\frac{\partial}{\partial r}\left(r\frac{\partial h}{\partial r}\right) - p_p\right) - \frac{K_p}{\mu_p r}\frac{\partial}{\partial r}\left(rh\frac{\partial p_p}{\partial r}\right) - \frac{\gamma}{3\mu}\frac{1}{r}\frac{\partial}{\partial r}\left\{r\left[(h^3 + 3\alpha\delta h^2)\frac{\partial}{\partial r}\left(\frac{1}{r}\frac{\partial}{\partial r}\left(r\frac{\partial h}{\partial r}\right)\right)\right]\right\}, \qquad [A.4]$$

where

$$\alpha = \frac{\mu}{\mu_p} < 1$$

according to (18). The latter equation describes the evolution of the spreading profile of the drop both in space and time. The only unknown dependence left is the pressure inside the porous layer, p_p.

The conservation law inside the porous layer

$$\frac{1}{r}\frac{\partial (rv)}{\partial r} + \frac{\partial u}{\partial z} = 0$$

is used to determine this pressure. The latter equation is integrated over z from $-\Delta$ to 0 inside the porous layer, using jump condition [A.2] and Darcy's law to express the velocity compoents using the pressure gradient. After some transformations

the final equation becomes

$$\frac{1}{r}\frac{\partial}{\partial r}\left(r\frac{\partial p_p}{\partial r}\right) - \frac{p_p}{\Delta\delta} = -\frac{\gamma}{r}\frac{\partial}{\partial r}\left\{r\left[\frac{h}{\delta}\frac{\partial}{\partial r}\left(\frac{1}{r}\frac{\partial}{\partial r}\left(r\frac{\partial h}{\partial r}\right)\right)\right]\right\} - \frac{1}{\Delta\delta}\frac{\gamma}{r}\frac{\partial}{\partial r}\left(r\frac{\partial h}{\partial r}\right), \quad [A.5]$$

which describes the radial distribution of the pressure inside the porous layer. Equation [A.5] shows that

(a) under the spherical part of the spreading drop the pressure inside the porous layer remains constant and equal to the pressure inside the drop, that is,

$$p_p^{\infty} = \frac{2\gamma\theta}{L}, \quad [A.6]$$

and, hence, the liquid does not flow at all inside the porous layer under the spherical part of the drop;

(b) the pressure inside the porous layer changes from the constant value [A.6] to the pressure outside the drop close to $r = L$ in a narrow region with a scale

$$\xi = \sqrt{\Delta\delta} \ll L, \quad [A.7]$$

as stated earlier (see Eqs. [7]–[9]).

Let us introduce a new local dimensionless variable, $\bar{x}$, as follows:

$$\bar{x} = \frac{r - L}{\xi}, \quad -\infty < \bar{x} < 0 \quad [A.8]$$

After small terms are omitted, Eq. [A.5] becomes

$$p_p'' - p_p = -\frac{\gamma\delta}{\xi^2}[(\bar{f}\,\bar{f}''')' + \bar{f}''], \quad [A.9]$$

where $\bar{f} = h/\delta$ is the dimensionless profile of the drop in this narrow transition region. The latter scale is selected in the same way as in part 1.

Equation [A.9] can be directly integrated using the following boundary conditions:

$$p_p(-\infty) = p_p^{\infty}, \quad [A.10]$$

$$p_p(0) = p_d. \quad [A.11]$$

The boundary condition [A.10] follows from Eq. [A.6], while condition [A.11] still includes the unknown pressure, p_d, which is determined below.

The solution of Eq. [A.9], which satisfies both boundary conditions [A.10] and [A.11], is

$$p_p = p_d e^{\bar{x}} + \frac{\gamma\delta}{\xi^3}\int_x^0 [(\bar{f}\,\bar{f}''')' + \bar{f}'']\sinh(\bar{x} - \bar{y})\,d\bar{y}. \quad [A.12]$$

Let us assume that

$$p_d \gg p_p^{\infty}. \quad [A.13]$$

This assumption means that the pressure inside the porous layer in the narrow region under consideration is much higher than the capillary pressure in the drop. The latter is reasonable to expect because just the pressure inside the porous layer determines the drop suction by the porous layer. In this case Eq. [A.12] reduces to

$$p_p = p_d e^{\bar{x}}. \quad [A.14]$$

To determine the unknown value, p_d, the solution for the pressure distribution inside the porous layer outside the drop [21], [24] is used. The solutions [21] and [A.14] should give the same radial velocity from both sides at $r = L$. Thus, we have

$$p_d = \frac{p_c}{1 + \frac{L}{\xi}\ln\frac{l}{L}} \approx p_c\frac{\xi}{L\ln\frac{l}{L}} \ll p_c. \quad [A.15]$$

The latter equation justifies the neglect of p_d relative to p_c in the main text above.

APPENDIX 2: LIST OF SYMBOLS

Latin

A, B, C	Integration constant
a	Radius of pores
d	Position of the front of the imbibition inside the porous layer at a horizontal imbibition
f	h/δ
g	Gravity acceleration
h	Thickness
K	Permeability of the porous layer
L	Radius of the drop base
l	Radius of the circular edge of the wetted region inside the porous layer
m	Porosity
p	Pressure
R	Radius of a sphere
r, z	Coordinate system
t, T	Time
u, v	Vertical and radial velocity components
V	Volume of the drop

Greek

α	$\mu/\mu_p < 1$
γ	Interfacial tension
Δ	Thickness of the porous layer
δ	Brinkman's length
λ	Small parameter
μ	Viscosity
θ	Dynamic contact angle
$\bar{\tau}, \bar{\chi}$	Dimensionless parameters (Eqs. [29] and [30])

ρ Density
ω Effective lubrication parameter
ξ Length scale of the narrow region close to the drop edge

Subscripts

0 Initial value
p Porous layer
c Capillary
g Gaseous phase
Δ Complete saturation of the porous layer in the vertical direction
μ Viscous
e Marks the constant value of the contact angle over the duration of the second stage
$+$ Expansion
— Shrinkage
d Drop
m Corresponds to the moment when the drop base reaches its maximum value
center Center of the sphere

Superscripts

$*$ Characteristic value
0 Liquid–porous layer interface
— Dimensionless
∞ Under the main part of the drop

ACKNOWLEDGMENTS

This research is sponsored by Grant GR/R 07578 from the U.K. Engineering and Physical Sciences Research Council and by Grant PB 96-599 from the Spanish Ministerio de Ciencia y Tecnologia.

REFERENCES

1. Starov, V. M., *Colloid J.* (USSR Academy of Sciences, English Translation) **45**(6), 1154 (1983).
2. De Gennes, P. G., *Rev. Mod. Phys.* **57,** 827 (1985).
3. Blake, T. D., and Hayenes, J. M., *J. Colloid Interface Sci.* **30,** 421 (1969).
4. Joanny, J.-F., *J. Mech. Theor. Appl.* **5,** 249 (1986).
5. Teletzke, G. F., Davis, T. H., and Scriven, L. E., *Chem. Eng. Commun.* **55,** 41 (1987).
6. Starov, V. M., Kalinin, V. V., and Chen, J.-D., *Adv. Colloid Interface Sci.* **50,** 187 (1994).
7. Tanigichi, M., Pieracci, J., and Belfort, G., *Langmuir* **17,** 4312 (2001).
8. Raphael, E., and de Gennes, P. G., *C. R. Acad. Sci. Paris Ser. II b* **327,** 685 (1999).
9. Aradian, A., Raphael, E., and de Gennes, P. G., *Eur. Phys. J. E* **2,** 367 (2000).
10. Bacri, L., and Brochard, F., *Eur. Phys. J. E* **3,** 87 (2000).
11. Beaverse, G., and Johns, D., *J. Fluid Mech.* **30**(1), 197 (1967).
12. Greenspan, H. P., *J. Fluid Mech.* **84,** 125 (1978).
13. Neogi, P., and Miller, C. A., *J. Colloid Interface Sci.* **92**(2), 338 (1983).
14. Davis, S. H., and Hocking, L. M., *Phys. Fluids* **11**(1), 48 (1999).
15. Davis, S. H., and Hocking, L. M., *Phys. Fluids* **12**(7), 1646 (2000).
16. Starov, V. M., Kosvintsev, S. R., Sobolev, V. D., Velarde, M. G., and Zhdanov, S. A., *J. Colloid Interface Sci.* **246**(2), 373 (2002).
17. Nayfeh, A. H., "Perturbation Methods." Wiley-Interscience, New York, 1973.
18. Starov, V. M., and Zhdanov, V. G., *Colloids surf.* **192,** 363 (2001).